

ALLOCATION OF TERRESTRIAL CARBON SOURCES USING $^{14}\text{CO}_2$: METHODS, MEASUREMENT, AND MODELING

Scott J Lehman¹ • John B Miller^{2,3} • Chad Wolak¹ • John Southon⁴ • Pieter P Tans² • Stephen A Montzka² • Colm Sweeney^{2,3} • Arlyn Andrews^{2,3} • Brian LaFranchi⁵ • Thomas P Guilderson⁵ • Jocelyn C Turnbull^{3,6}

ABSTRACT. The radiocarbon content of whole air provides a theoretically ideal and now observationally proven tracer for recently added fossil-fuel-derived CO_2 in the atmosphere (C_{ff}). Over large industrialized land areas, determination of C_{ff} also constrains the change in CO_2 due to uptake and release by the terrestrial biosphere. Here, we review the development of a $\Delta^{14}\text{CO}_2$ measurement program and its implementation within the US portion of the NOAA Global Monitoring Division's air sampling network. The $\Delta^{14}\text{CO}_2$ measurement repeatability is evaluated based on surveillance cylinders of whole air and equates to a C_{ff} detection limit of ≤ 0.9 ppm from measurement uncertainties alone. We also attempt to quantify additional sources of uncertainty arising from non-fossil terms in the atmospheric $^{14}\text{CO}_2$ budget and from uncertainties in the composition of "background" air against which C_{ff} enhancements occur. As an example of how we apply the measurements, we present estimates of the boundary layer enhancements of C_{ff} and C_{bio} using observations obtained from vertical airborne sampling profiles off of the northeastern US. We also present an updated time series of measurements from NOAA GMD's Niwot Ridge site at 3475 m asl in Colorado in order to characterize recent $\Delta^{14}\text{CO}_2$ variability in the well-mixed free troposphere.

INTRODUCTION

The small radiocarbon fraction of total CO_2 has proven to be an ideal tracer for its fossil-fuel-derived component (cf. Levin et al. 2003; Turnbull et al. 2006; Graven et al. 2009; Miller et al. 2012). Unlike all other contributions to the atmospheric CO_2 budget, the fossil fuel component is devoid of ^{14}C , so that temporal and spatial gradients in recently added fossil fuel CO_2 can be readily identified as ^{14}C gradients provided there is adequate precision in the measurements. Over large industrialized land areas such as Eurasia and North America, the use of ^{14}C to isolate the contribution of recently added fossil-fuel-derived CO_2 to the observed CO_2 mole fraction (C_{ff}) also quantifies (by difference) the change in atmospheric CO_2 due to uptake and release by the terrestrial biosphere (C_{bio}). Here, we review the development of a precise $^{14}\text{CO}_2$ processing and measurement capability in discrete ~ 2 -L (STP) samples of whole air, suitable for implementation within existing flask sampling networks around the world. Our development effort was undertaken as a collaboration between the University of Colorado, the Global Monitoring Division (GMD) of NOAA's Earth System Research Laboratory, and the Keck AMS Facility at the University of California at Irvine. Most of our measurements occur within NOAA GMD's global air sampling network, which includes flask sampling at the surface, in aircraft profiles, and from tall towers (<http://www.esrl.noaa.gov/gmd/dv/iadv/>). Paired $\Delta^{14}\text{CO}_2$ and trace gas measurements expanded into a growing network of tall towers around the US between 2009 and 2010, facilitated in part by a new measurement collaboration with the Center for Accelerator Mass Spectrometry at Lawrence Livermore National Laboratory.

¹Institute of Arctic and Alpine Research, University of Colorado, Boulder, Colorado, USA.

²NOAA Earth System Research Laboratory, Boulder, Colorado, USA.

³Cooperative Institute for Research in Environmental Sciences, University of Colorado, Boulder, Colorado, USA.

⁴Keck AMS Facility, University of California, Irvine, California, USA.

⁵Lawrence Livermore National Lab, Livermore, California, USA.

⁶National Isotope Centre, GNS Science, Lower Hutt, New Zealand.

We begin by presenting the atmospheric budgets of CO₂ and Δ¹⁴CO₂ and an analytical framework for C_{ff} detection using paired CO₂ and Δ¹⁴CO₂ observations. We then document the Δ¹⁴CO₂ measurement repeatability as ascertained in surveillance cylinders of whole air and give an example of how authentic field measurements have been used to partition boundary layer enhancements of CO₂ into fossil fuel and terrestrial biospheric components. Finally, we describe uncertainties in our C_{ff} detection methods arising from non-fossil terms in the isotopic budget and from incomplete representation of “background” air against which enhancements are determined.

C_{ff} DETECTION USING ¹⁴CO₂

The value of ¹⁴C measurements with regard to C_{ff} detection arises from the fact that ancient carbon comprising fossil fuels is devoid of ¹⁴C due to radiodecay, while the ¹⁴C activity of the atmosphere and living biosphere is maintained at relatively high (i.e. “modern”) levels as a result of ongoing ¹⁴C production. Thus, CO₂ sourced from the combustion of fossil fuels is ¹⁴C-free whereas all other sources of CO₂ to the atmosphere have isotopic signatures that are close to that of the atmosphere itself. In simplified form, Δ¹⁴C = [(¹⁴C/C)_{sample} / (¹⁴C/C)_{standard} - 1]1000‰, but with corrections for mass-dependent fractionation (from δ¹³C measurement) and small amounts of radioactive decay between the times of sampling and measurement (see Stuiver and Polach 1977 for full expression). Therefore, the Δ¹⁴CO₂ of fossil fuel CO₂ = -1000‰. In contrast, the measured value of the recent, well-mixed atmosphere is about +50‰ (Turnbull et al. 2007; Levin et al. 2008; Graven et al. 2012). By mass balance, the addition of 1 ppm of fossil CO₂ to an atmospheric CO₂ burden of 390 ppm will produce a Δ¹⁴C depletion of ~2.7‰ (i.e. (-1000‰ - 50‰)/390 ppm).

We describe the global atmospheric budgets for CO₂ and its ¹⁴C:C ratio (expressed in the Δ notation) below in Equations 1a and b:

$$\frac{dC_{atm}}{dt} = F_{bio} + F_{oce} + F_{fos} \quad (1a)$$

$$C_{atm} \frac{d\Delta_{atm}}{dt} = (\Delta_{fos} - \Delta_{atm})F_{fos} + \Delta_{ocedis}F_{ocedis} + \Delta_{biodis}F_{biodis} + isoF_{nuc} + isoF_{cosmo} \quad (1b)$$

For the CO₂ budget (Equation 1a), C_{atm} refers to the atmospheric mole fraction of CO₂, F_{bio} represents the net terrestrial biosphere-atmosphere flux, F_{oce} is the net ocean-atmosphere flux, and F_{fos} is the flux from fossil fuel combustion. For the isotopic budget (Equation 1b), net isotopic exchange terms can be neglected since the Δ notation includes a δ¹³C correction that accounts for mass dependent fractionation. The subscripts *ocedis* and *biodis* respectively denote the ocean-atmosphere and biosphere-atmosphere isotopic disequilibria and associated gross (one-way) mass fluxes. Isotopic disequilibrium refers to the difference between isotopic signatures of carbon leaving and entering a reservoir. In the terrestrial case, disequilibrium results from the respiration of ¹⁴C-enriched CO₂ assimilated, on average, a decade or two ago when the atmospheric Δ¹⁴C was much higher as a result of atmospheric nuclear weapons testing. In the oceanic case, it results from the re-emergence of aged ¹⁴C-depleted CO₂ at the surface, carried by waters that have been out of contact with the atmosphere long enough for radioactive decay to become significant. The subscript *nuc* refers to the flux of ¹⁴CO₂ from nuclear reactors, and *cosmo* to the cosmogenic production of ¹⁴C. These last terms are pure ¹⁴C fluxes and as such do not have isotopic signatures and are represented only as “iso”-fluxes. If the non-fossil contributions to the tropospheric ¹⁴C budget are either small or relatively uniform in space, then the mass balance sensitivity and the ¹⁴C measurement precision will closely approximate the actual C_{ff} detection capability.

Allocation of Terrestrial C Sources Using $^{14}\text{CO}_2$

To illustrate this, we show in Figure 1 a map of wintertime fossil-fuel-derived CO_2 and (total) $\Delta^{14}\text{CO}_2$ within the planetary boundary layer (PBL) over North America as represented in the TM5 transport model (Krol et al. 2005; Miller et al. 2012). For $^{14}\text{CO}_2$, all terms in Equation 1b are represented in the model, except the nuclear term (cf. Graven and Gruber 2011). The color scales depicting $\Delta^{14}\text{CO}_2$ and fossil fuel CO_2 distributions correspond to the expected mass balance sensitivity of $-2.7\text{‰}/\text{ppm}$. Thus, the similar colors and patterns in Figure 1 indicate that, over North America, the ^{14}C gradients are controlled largely by the presence of fossil fuel CO_2 . The remaining small differences are due primarily to small atmospheric gradients imposed by the terrestrial disequilibrium flux of ^{14}C ($\Delta_{\text{biadis}}F_{\text{biadis}}$ in Equation 1b). This contribution can be quantified and applied as a small correction in the fossil fuel CO_2 detection algorithm, as discussed below. ^{14}C emissions from nuclear power generation (Graven and Gruber 2011), which are neglected in this simulation due to their large relative uncertainty, may produce near-surface signals averaging 1–2‰ in the densely populated northeastern US (see below for a discussion of related C_{ff} detection uncertainties). The cosmogenic production and ocean disequilibrium terms do not result in significant gradients of ^{14}C over the US, although they are also specified in the model. Isotopic budget terms used in the TM5 simulations have been estimated following methods outlined in Turnbull et al. (2009) and at CarbonTracker (<http://www.esrl.noaa.gov/gmd/ccgg/carbontracker/documentation.html>).

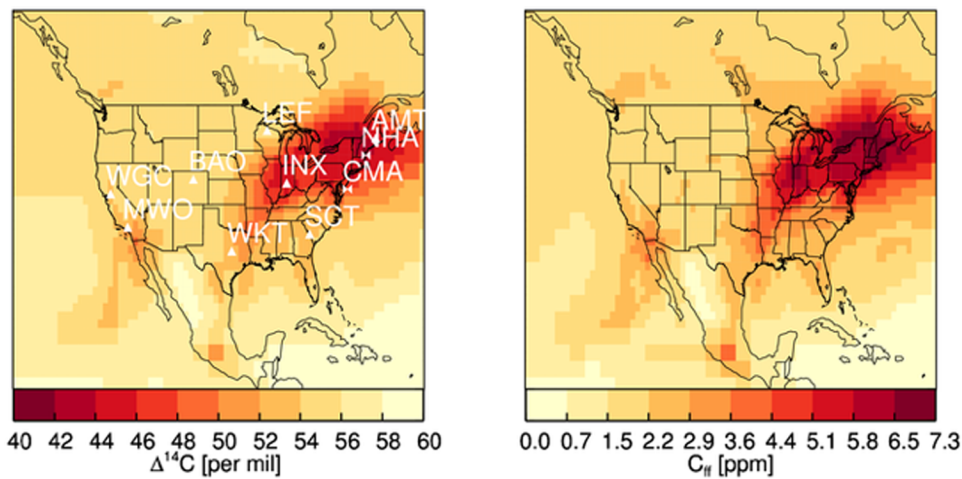


Figure 1 a) $\Delta^{14}\text{CO}_2$ (left panel) and b) the fossil fuel component of total CO_2 (C_{ff} ; right panel) in the atmosphere near the surface over North America for a week in January 2006 in the TM5 transport model. The CO_2 and $^{14}\text{CO}_2$ budget terms are discussed in the text and at <http://www.esrl.noaa.gov/gmd/ccgg/carbontracker/documentation.html>. The fossil fuel emissions used in the model are based on the CDIAC US and global totals (Boden et al. 2009), with US national seasonality (Blasing et al. 2005), and spatial patterns from the EDGAR version 4.0 inventory (http://edgar.jrc.ec.europa.eu/archived_datasets.php). Existing ^{14}C sampling sites for the US are given in a) according to site code (as at <http://www.esrl.noaa.gov/gmd/dv/iadv/>). Bowties are aircraft sites and triangles are surface or tower sites. NWR (surface flask site) was excluded for clarity, but overlies BAO. Measurements at BAO, LEF, and AMT are made in collaboration with investigators at LLNL.

In order to quantify the fossil fuel CO_2 signal from measurements, we follow Levin et al. (2003) in considering observations of both CO_2 and $\Delta^{14}\text{C}$ to be the sum of background values for each tracer plus any fossil fuel and biospheric contributions:

$$C_{\text{obs}} = C_{\text{bg}} + C_{\text{ff}} + C_{\text{bio}} \quad (2a)$$

$$\Delta_{\text{obs}}C_{\text{obs}} = \Delta_{\text{bg}}C_{\text{bg}} + \Delta_{\text{ff}}C_{\text{ff}} + \Delta_{\text{bio}}C_{\text{bio}} \quad (2b)$$

As in Turnbull et al. (2006), we divide C_{bio} into photosynthetic and respiratory terms C_{photo} and C_{resp} , respectively. Expanding and combining Equations 2a and b, and setting Δ_{photo} equal to Δ_{bg} (which will be the same as a result of $^{13}\text{C}:^{12}\text{C}$ normalization), we obtain

$$C_{ff} = \frac{C_{obs}(\Delta_{obs} - \Delta_{bg})}{\Delta_{ff} - \Delta_{bg}} - \frac{C_{resp}(\Delta_{resp} - \Delta_{bg})}{\Delta_{ff} - \Delta_{bg}} \quad (2c)$$

In Equation 2c, all of the quantities in the first term on the right-hand side are either known *a priori* or can be measured, and the second term, which we call C_{corr_resp} , is a correction to C_{ff} , which accounts for the disequilibrium contribution of ^{14}C from heterotrophic respiration. The recent isotopic disequilibrium is approximately the difference between present-day atmospheric $\Delta^{14}\text{C}$ and that from a decade or so earlier (Ciais et al. 1999), reflecting the mean residence time of carbon in the terrestrial biosphere. C_{corr_resp} , which always acts to lower C_{ff} , was estimated previously as 0.4–0.8 ppm in summer and 0.2–0.3 ppm in winter, based on estimates of the seasonally varying heterotrophic respiration flux and PBL height and the mean terrestrial biosphere isotopic disequilibrium (Turnbull et al. 2006, 2009). Miller et al. (2012) recently introduced a method for estimating the C_{corr_resp} correction term on a sample-by-sample basis, which we will discuss below.

Having estimated C_{corr_resp} , the C_{ff} enhancement relative to background is calculated from Equation 2c. Equation 2a can then be applied to isolate C_{bio} , which is the biological enhancement or depletion of CO_2 relative to background.

$^{14}\text{CO}_2$ MEASUREMENT PRECISION AND C_{ff} DETECTION LIMIT

Taking the simulated distribution of $\Delta^{14}\text{CO}_2$ in the near surface over the US (for a week in January 2006) in Figure 1a as an example, we may expect continental-scale gradients within the PBL of up to 10–15‰ in winter. Hsueh et al. (2007) document comparable gradients over the US in summer, based on measurements in corn. Thus, a $\Delta^{14}\text{CO}_2$ measurement precision of better than 2‰ would be needed in order to resolve synoptic gradients with confidence (i.e. with a signal to noise ratio of $\geq 5:1$). Time-dependent $\Delta^{14}\text{CO}_2$ variability within the PBL at observing sites in the US, Europe, and East Asia may reach 10–20‰ (cf. Levin et al. 2003; Turnbull et al. 2011; Miller et al. 2012) but is often much less, depending on transport and proximity of observing sites to major fossil CO_2 combustion sources. We also see from Equations 2a–c that quantification of fossil fuel CO_2 enhancements from observations requires measurements in both “background” and “observed” air for both the CO_2 mole fraction and its ^{14}C activity. Propagation of measurement uncertainties through Equation 2c suggests that in order to obtain a C_{ff} detection limit of ≤ 1 ppm (1σ), the necessary $\Delta^{14}\text{CO}_2$ measurement precision will be $\leq 2\text{‰}$ (1σ), with the C_{ff} detection limit determined almost entirely by the much larger relative uncertainty in the ^{14}C measurement precision (i.e. $\sim 1/20$ for ^{14}C vs $\sim 1/4000$ for CO_2 if the CO_2 measurement precision is ± 0.1 ppm; Conway et al. 1994). For long-term monitoring programs, the relevant metric of precision will be the long-term ^{14}C measurement repeatability (defined by JCGM 2008) in appropriate control materials rather than the single-sample measurement precision (sometimes also called the “external precision” when using AMS).

At the University of Colorado, the long-term measurement repeatability is evaluated based on repeat extraction and measurement of whole air from control cylinders. From 2003 to 2009, we used for this purpose a single cylinder of whole air filled at NOAA’s Niwot Ridge, Colorado site (NWR, at 3475 m asl) in September 2002, which we refer to as “NWTstd” (Turnbull et al. 2007). In 2009, by which time NWTstd was near exhaustion, we introduced 2 new control cylinders, NWT3 and NWT4. Both were filled at NWR in February 2009, but a small amount of ^{14}C -free CO_2 was added

Allocation of Terrestrial C Sources Using $^{14}\text{CO}_2$

to NWT4 to lower the activity with respect to ambient values. Presently, we measure 3 extraction aliquots each from NWT3 and NWT4 in each AMS measurement wheel. Individual measurement wheels are typically comprised of 8 primary measurement standards (NBS oxalic acid I, Ox-I), 1 secondary standard (NBS oxalic acid II, Ox-II), 1 process blank (^{14}C -free CO_2 in air from cylinders), 6 controls (NWT3 and 4), and 24 authentic samples. Extraction, graphitization, measurement and normalization follow methods described in Turnbull et al. (2007). Extraction occurs on either a manual or an automated extraction line (“CRex,” as described in Turnbull et al. 2010) and samples from individual observing sites are always extracted on the same line.

In Figure 2, we show individual measurement values, means and 1σ repeatabilities for both NWT3 and 4 by order of either measurement or extraction, from September 2009 to May 2012. There is no statistically significant difference between results for the 2 extraction lines. Temporal patterns of the measured value by measurement order suggest some systematic variances result from either graphitization or measurement conditions (graphitization and measurement occur nearly simultaneously). This may be expected, despite the large number of accompanying primary measurement standards, since the within-wheel agreement of controls from gas cylinders is generally better than that for Ox-I (Graven et al. 2007; Lehman et al. 2011).

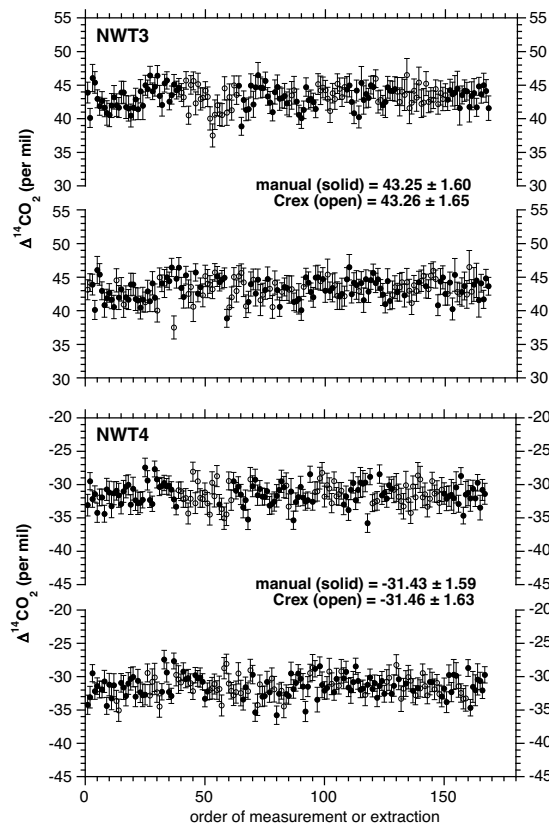


Figure 2 $\Delta^{14}\text{CO}_2$ measurement values in individual extraction aliquots of NWT3 or NWT4, by order of graphitization and measurement (upper series) or extraction (lower series). “Manual” (solid symbols) and “CRex” (open symbols) refer to results for manual and automated extraction lines, respectively. Uncertainties for each series are given at 1σ , and define the long-term repeatability of the measurement, as discussed in the text.

Long-term repeatabilities for NWT3 and 4 of 1.6–1.7‰ (Figure 2) are slightly better than the values of 1.8–1.9‰ previously reported for NWTstd measured between 2003 and 2009 (Turnbull et al. 2007; Lehman et al. 2011). For authentic samples, we continue to report a 1σ measurement repeatability of $\pm 1.8\%$ or the single-sample measurement precision, whichever is larger (Turnbull et al. 2007). Propagation of uncertainties of $\pm 1.8\%$ for $\Delta^{14}\text{CO}_2$ and of ± 0.1 ppm for CO_2 through Equation 2c suggests a long-term detection limit for C_{ff} of 0.9 ppm, based on measurement uncertainties alone. This will also characterize the uncertainty in C_{bio} determined according to Equation 2a.

A NORTHEAST US EXAMPLE

As an example of how we apply actual field measurements, we show in Figure 3 the separation of boundary layer enhancements of CO_2 into their fossil fuel and biological components, using ~ 6 yr of airborne observations at CMA and NHA (from Miller et al. 2012), in a region of significant emissions and air outflow in the northeast US (see Figure 1 for site locations). In this analysis, boundary layer samples from ~ 300 m asl are treated as *obs*, and *bg* is from ~ 4000 m asl within the well-mixed free troposphere sampled in the same vertical profile. This treatment of the observations effectively assumes that the overlying free troposphere is the source of air into which new emissions are added in the PBL. The presentation in Figure 3 differs from that in Miller et al. (2012) in that here we decompose only the observations from ~ 300 m asl, as opposed to those from ~ 300 m asl and from 2000–2400 m asl, since the latter are often above the PBL.

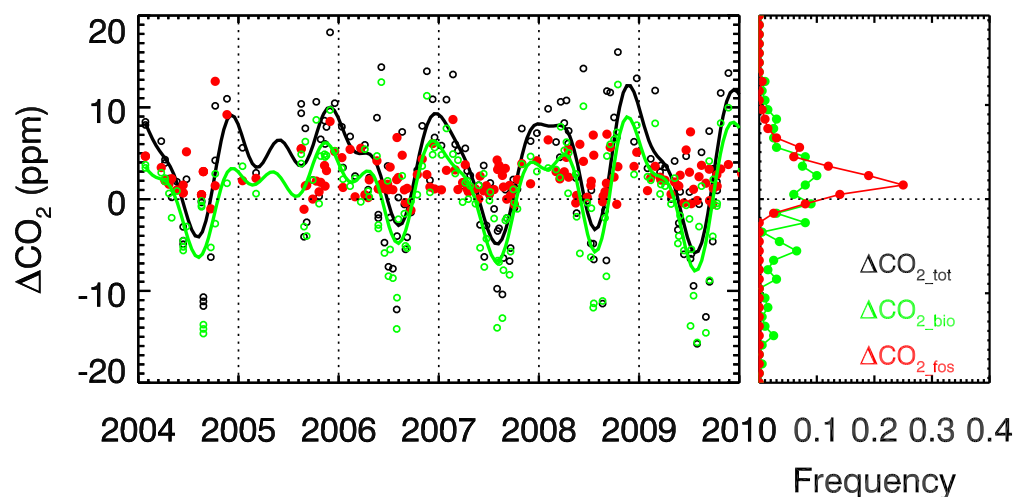


Figure 3 Enhancement or depletion of CO_2 in the planetary boundary layer (from ~ 300 m asl) relative to the free troposphere (~ 4000 m asl) in 6 yr of approximately biweekly airborne profiles at CMA and NHA (Figure 1a), separated into biogenic (green) and fossil (red) fractions according to Equations 2a–c. Black and green lines highlight, respectively, the seasonal variation of raw CO_2 enhancement or depletion in the boundary layer and that attributable to biospheric exchange. The occasional negative values of C_{ff} arise primarily from vertical $\Delta^{14}\text{CO}_2$ gradients that are within measurement uncertainties and to a far lesser extent from errors inherent in our simple one-dimensional analytical model.

We see that C_{ff} is present within the PBL throughout the year, with $\sim 80\%$ of the observations in the range of 0–7 ppm. Occasional instances of negative C_{ff} , which are non-physical, are explained almost entirely by the 1σ $\Delta^{14}\text{CO}_2$ measurement uncertainty, and to a far lesser extent by the failure of our simplified assumptions regarding the source of “background” air (Miller et al. 2012). Accounting explicitly for C_{ff} using ^{14}C also sharpens our view of the biospheric CO_2 signal, which

differs significantly from the raw boundary layer enhancement or depletion of CO_2 (i.e. the difference between green and black lines in Figure 3). Also noteworthy is the large presence of respiratory CO_2 in the boundary layer in winter, when, on average, the biological emissions account for $\sim 60\%$ of the total PBL CO_2 enhancement. This suggests that reliable attribution of sources using ground- or satellite-based, CO_2 -only observing strategies will not be possible without additional information from proven C_{ff} tracers such as ^{14}C , even over urban and industrial areas in winter.

UNCERTAINTIES FROM CORRECTION TERMS

In the analysis above, the correction term C_{corr_resp} (the 2nd term in Equation 2c) was calculated explicitly for each sample according to methods detailed in Miller et al. (2012). We use these estimates here as a quantitative basis for assessing related uncertainties in C_{ff} . The heterotrophic respiration flux as a function of time since assimilation was estimated monthly at a resolution of $1^\circ \times 1^\circ$ using pulse response functions from the CASA biosphere model (Thompson and Randerson 1999) and then convolved with the atmospheric $\Delta^{14}\text{CO}_2$ history (cf. Levin and Kromer 2004) to obtain $F_{biodis}\Delta_{bios}$ (Equation 1b). This was applied to the individual observations (as the numerator in C_{corr_resp}) using spatial sensitivities to surface emissions obtained for each sample from a Lagrangian transport model (FLEXPART, Stohl et al. 2005). The individual corrections along with their monthly mean and standard deviation for all observations at CMA are given in Figure 4 (from Miller et al. 2012). As expected, the estimates for the $\sim 300\text{-m-asl}$ observations within the PBL show a larger sensitivity to the surface emissions than the samples from $2000\text{--}2400\text{ m asl}$. The monthly average estimates for the PBL of $\sim 0.7\text{ ppm}$ in summer and $\sim 0.3\text{ ppm}$ in winter are comparable to previous estimates of the seasonal mean corrections (Turnbull et al. 2006, 2009). The likely uncertainty associated with applying seasonal mean corrections as opposed to explicitly determined sample-by-sample corrections is indicated by the monthly 1σ standard deviations (up to $\sim 0.4\text{ ppm}$ in summer and $\sim 0.1\text{ ppm}$ in winter). Associated corrections and uncertainties will likely be smaller for regions dominated by relatively dry Mediterranean climates compared to those for the humid continental eastern US that apply here. The absolute uncertainty is difficult to determine, but will stem primarily from the accuracy of the biospheric residence times in the CASA biosphere model.

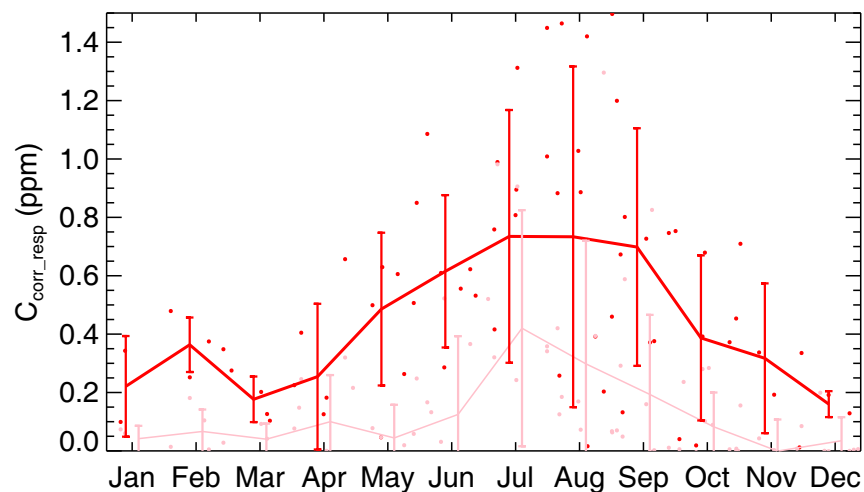


Figure 4 Estimates of C_{corr_resp} for individual $\sim 300\text{-m-asl}$ (dark red) and $2000\text{--}2400\text{-m-asl}$ (light red) samples at CMA, from Miller et al. (2012). The monthly means and standard deviations are also shown.

As stated earlier, we have neglected the influence of $^{14}\text{CO}_2$ emissions from the nuclear power sector in the TM5 simulations and in Equation 2c, which is used to determine C_{ff} from observations. Using gridded estimates of the nuclear emissions from Graven and Gruber (2011), we calculate possible corrections for all observations at CMA using the same method as above. Like C_{corr_resp} , the term C_{corr_nuc} will always act to raise C_{ff} , since both are surface sources of $^{14}\text{CO}_2$ that mask the isotopic dilution associated with surface emissions of fossil-fuel-derived CO_2 . As shown in Figure 5, estimated C_{corr_nuc} shows little seasonal variation and is considerably larger in the near surface than at 2000–2400 m asl. Monthly means range from 0.25–0.9 ppm for the PBL, with monthly 1σ standard deviations of 0.15–1.0 ppm. Estimates of C_{corr_nuc} and its monthly standard deviation for all observations at NHA (not shown) are approximately 50% lower. The annual mean signals agree within errors with those for the northeast US obtained by Graven and Gruber (2011) (using an Eulerian transport model) for their central estimates of nuclear emissions. The predicted gradient in nuclear signals between CMA and NHA is due to the distribution of reactors (there are substantially fewer in northern New England than in the large metropolitan areas to the south and west; <http://www.nrc.gov/reactors/operating/map-power-reactors.html>) and the approximate e-folding length scale for sensitivity to emissions influencing our 300-m-asl observations at CMA and NHA of 150–300 km (from FLEXPART).

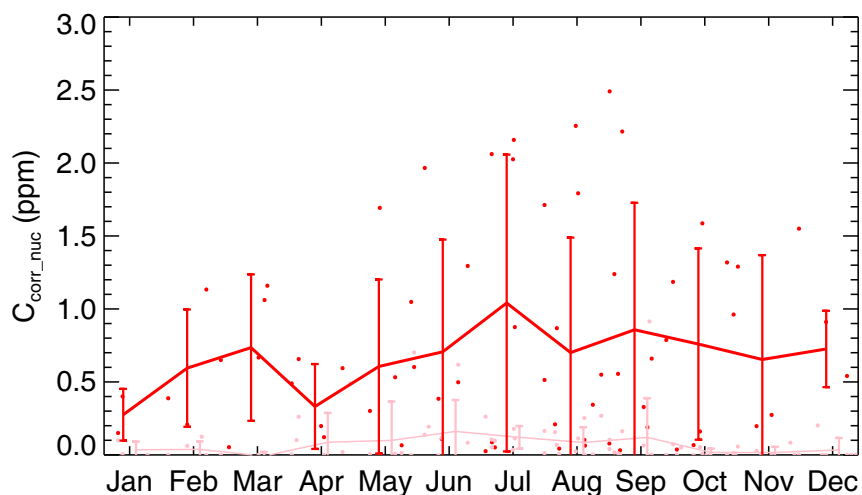


Figure 5 Estimates of C_{corr_nuc} for individual ~ 300 -m-asl (dark red) and 2000–2400-m-asl (light red) samples at CMA, using central, gridded estimates of US nuclear $^{14}\text{CO}_2$ emissions from Graven and Gruber (2011). The method of calculation is otherwise the same as for C_{corr_resp} (Figure 4). The monthly means and standard deviations are also shown.

If the central emissions estimates of Graven and Gruber (2011) closely approximate the actual power plant emissions of $^{14}\text{CO}_2$, then we may conclude that likely maximum uncertainties in C_{ff} due to variability in C_{corr_nuc} are in the range of 0.1 to 1.0 ppm for the eastern US (based on estimates for CMA, influenced by a region in which reactors are relatively common). The potential low bias in C_{ff} that arises from neglecting C_{corr_nuc} altogether has about the same range as the uncertainty (e.g. range of monthly means compared to range of monthly standard deviations in Figure 5). It is important to note, however, that the $^{14}\text{CO}_2$ emissions estimates are characterized by large uncertainties, which Graven and Gruber (2011) represent as 70% confidence intervals of the distributions of total ^{14}C emissions for different reactor types. In the US, all reactors are either pressurized- or boiling-water reactors, both of which emit ^{14}C as $^{14}\text{CO}_2$, although emissions from the more common pres-

surized-water reactors (PWRs) are primarily in the form of methane. Estimates of the fraction of ^{14}C emitted as $^{14}\text{CO}_2$ for PWRs range from 5–25% (IAEA 2004), which suggests substantial uncertainty in overall nuclear $^{14}\text{CO}_2$ emissions in the US. Estimates of the influence on C_{ff} for the lower limit of the 70% confidence interval for nuclear emissions are ≤ 0.25 ppm for the US (Graven and Gruber 2011). The influence associated with the upper limit of emissions estimates for the US is large enough to produce frequent and sustained reversals in the vertical ^{14}C gradient that are not observed (i.e. producing negative C_{ff} -well in excess of that in Figure 3). The distributions used to obtain 70% confidence limits may, in fact, contain a high bias, as the fraction of ^{14}C emitted as $^{14}\text{CO}_2$ by PWRs was specified as 25%, which is at the upper end of independent estimates (IAEA 2004).

Regardless of the uncertainties, the nuclear signal in much of the central and western US will be negligible (with the possible exception of areas near 4 reactors in southern California and 3 in Arizona). In parts of Europe, Canada, and Japan, the necessary corrections and uncertainties will be substantially larger due to the large number of reactors and reactor types, and the presence of fuel reprocessing plants (Levin et al. 2003; Graven and Gruber 2011). For ^{14}C -based C_{ff} observing programs in these areas, and very near reactor sites in the US, additional monitoring of nuclear $^{14}\text{CO}_2$ emissions may be needed (Graven and Gruber 2011; Balter 2012).

UNCERTAINTIES FROM SPECIFICATION OF “BACKGROUND”

Determination of the enhancement of fossil-fuel-derived CO_2 directly from observations requires measurements and/or estimates of both “observed” and “background” air (i.e. Equations 2a–c). In the case of the NE US example given above, measurements from the overlying free troposphere sampled in the same vertical profile as the PBL “observation” were used to represent “background.” However, if air refreshing the PBL (into which new emissions are then added) originates from locations with a different CO_2 mole fraction and/or a different isotopic composition than the contemporaneously overlying free troposphere, the estimated PBL enhancement would be subject to error over and above that associated with measurement uncertainty alone. In the case of seasonally persistent horizontal shear (in which upper and lower level air originate from different locations), such errors would be present as an undetected seasonal bias in C_{ff} .

Sustained meridional gradients of $\Delta^{14}\text{CO}_2$ in the free troposphere over Northern Hemisphere continents are expected as a result of the changing balance of isotopic budget terms (primarily *fos* and *biodis* terms in Equation 1b) with latitude (Randerson et al. 2002; Levin et al. 2010; Graven et al. 2012), while strong upper level westerly winds will tend to suppress zonal free troposphere $\Delta^{14}\text{CO}_2$ gradients in middle latitudes. For the period 2005–2007 (the most recent available observations), Graven et al. (2012) document a mid-latitude minimum in average $\Delta^{14}\text{CO}_2$ in the Northern Hemisphere of $\sim 3 \pm 1\text{‰}$ with respect to observations at 15°N and of $\sim 1 \pm 0.5\text{‰}$ with respect to 70°N . These are comparable to mean Northern Hemisphere gradients observed by Levin et al. (2010) from 1994–1997, but in both studies the NH gradient is characterized by only 4 observing sites.

For the NE US example, Miller et al. (2012) provide an analysis of possible bias resulting from seasonal shear along the east coast based on simulated $\Delta^{14}\text{CO}_2$ distributions over North America, since the actual recent $\Delta^{14}\text{CO}_2$ distribution remains poorly constrained. Back-trajectories calculated by FLEXPART for CMA in summer show that the high-altitude samples originate further north by $\sim 15^\circ$ than do those for the lower troposphere 3 days prior to sampling. Sampling the TM5 $\Delta^{14}\text{C}$ output using the end-points of 7-day back trajectories indicates that the trajectories for upper-level samples intersect simulated free troposphere $\Delta^{14}\text{C}$ values higher than those for the lower-level samples by $\sim 1.6\text{‰}$, equating to a possible seasonal C_{ff} bias of $\sim +0.5$ ppm C_{ff} . During winter, the difference between upper- and lower-level end-points is $\sim 3^\circ$ of latitude 3 days prior to sampling, suggesting

that the contemporaneously overlying wintertime free troposphere provides a relatively reliable estimate of background.

We can evaluate the mean and variability of the recent zonal free troposphere $\Delta^{14}\text{CO}_2$ gradient over North America by comparing measurement results from NWR (3475 m asl, 40.05°N) and upper-level (~4000 m asl) samples from CMA (38.83°N) and NHA (42.95°N) for the same time periods. In Figure 6a, we show an updated $\Delta^{14}\text{CO}_2$ time series for NWR for the period 2004–2011 (extending results in Turnbull et al. 2007), with observations associated with $>+2\sigma$ outliers in corresponding measurements of carbon monoxide removed in order to reduce the influence of local pollution events. Also given is a combined polynomial and harmonic fit to the observations that is frequently used to isolate the seasonal signal in atmospheric CO_2 observations (Thoning et al. 1989). The 1σ deviation of the individual NWR observations from the fit is $\pm 1.9\text{‰}$, similar to the long-term measurement uncertainty.

In Figure 6b, we compare the individual ~4000-m-asl observations from CMA and NHA (from Miller et al. 2012) to the NWR fitted curve. The mean deviation of the NHA observations from the NWR fit is $+0.07\text{‰}$, with a 1σ deviation from the NWR fit of $\pm 2.2\text{‰}$, comparable to that for the NWR observations themselves. For CMA, the mean and 1σ standard deviations with respect to the NWR fit are $+0.61\text{‰}$ and $\pm 2.6\text{‰}$, respectively. Positive deviations of the individual observations with respect to NWR occur at both eastern sites in summer (Figure 6b), possibly due to weaker summertime mean westerlies and increased zonal flow. The shared variability at different sites sampling the relatively well-mixed free troposphere likely arises from changes in vertical transport in addition to seasonal changes in sources (Turnbull et al. 2009).

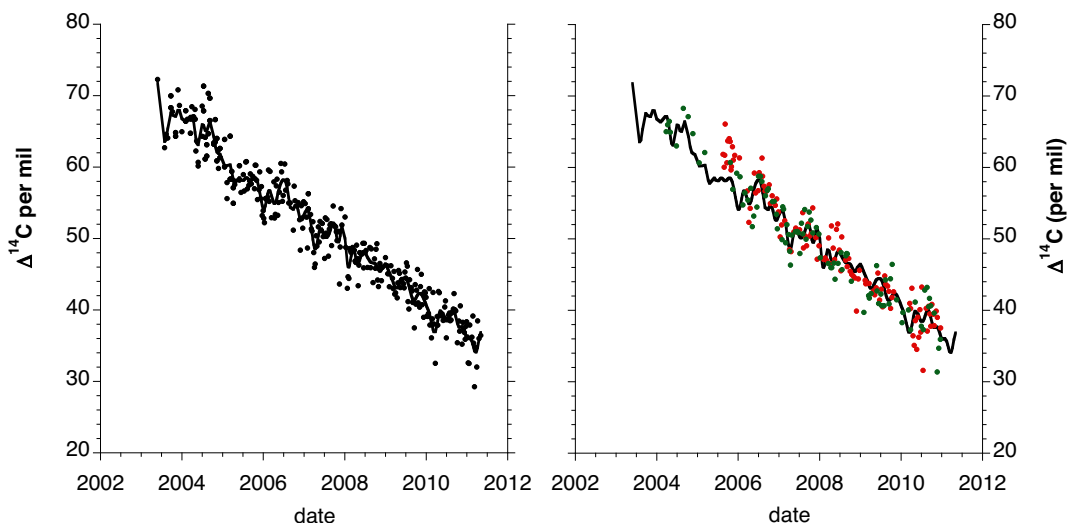


Figure 6 a) $\Delta^{14}\text{CO}_2$ measurement values at NWR, Colorado (3475 m asl, 40.5°N), for 2003 through 2011. Results up to 17 Jan 2006 were presented earlier by Turnbull et al. (2007). Measurements for which corresponding carbon monoxide values exceeded a seasonal fit by $>+2\sigma$ were removed to reduce the influence of local pollution events on the record. Remaining results were fitted (black curve) according to the method of Thoning et al. (1989). Individual measurement uncertainties are not shown for clarity, but are discussed in the text and listed in Table S1 (Supplementary file accompanying the online version of this article). b) $\Delta^{14}\text{CO}_2$ measurement values for ~4000 m asl samples at NHA (green) and CMA (red), compared to the fitted curve for NWR in (a). Site locations are given in Figure 1a. Note that prior to 24 Aug 2004 at NWR, pilot measurements were made at Rafter Radiocarbon Lab (Turnbull et al. 2007).

Allocation of Terrestrial C Sources Using $^{14}\text{CO}_2$

From the gradients described above, assumed “background” $\Delta^{14}\text{CO}_2$ may differ from actual background by as much as 1.5–3‰ (i.e. ~ 0.5 – 1 ppm C_{ff}) for large-scale, regional studies. In the case of relatively localized campaigns for which up- and down-wind observations within the PBL may be available, the background uncertainty will be much less and limited primarily by the measurement precision. We note that recent build-out of the observing network in the US, which now includes \sim thrice weekly measurements at 9 tall towers (Figure 1a), provides the opportunity to develop a spatially and temporally continuous estimate of the $\Delta^{14}\text{CO}_2$ field over the US using numerical transport models guided by observations. This, we expect, will substantially reduce both uncertainty and potential bias in C_{ff} arising from uncertainty in “background.”

CONCLUSIONS

We have demonstrated a scientifically meaningful $\Delta^{14}\text{CO}_2$ measurement capability in small (~ 2 L) samples of whole air suitable for implementation within flask sampling networks around the world. The measurement repeatability in extraction aliquots of whole air from surveillance cylinders is $\leq 1.7\%$ (1σ) since 2009, and 1.8% (1σ) since the inception of our measurement programs in 2003. The latter equates to a fossil fuel CO_2 (C_{ff}) detection capability of 0.9 ppm from measurement uncertainty alone, with an equivalent uncertainty in estimates of the change in CO_2 due to biological uptake and release (C_{bio}). Additional sources of uncertainty in the ^{14}C -based detection of C_{ff} arise from “non-fossil” terms in the isotopic budget, primarily the return flux of $^{14}\text{CO}_2$ to the atmosphere from heterotrophic respiration and $^{14}\text{CO}_2$ emissions from the nuclear power industry. For the eastern US, we estimate uncertainties from the heterotrophic respiration term of $\sim \pm 0.4$ ppm C_{ff} in summer (and substantially less in winter), when specifying seasonal-mean rather than sample-by-sample corrections. Uncertainties associated with variable emissions from the nuclear power sector in the eastern US have a likely range of ± 0.1 to ± 1.0 ppm C_{ff} , with a comparable range in the maximum bias in C_{ff} to lower-than-actual values if these emissions are neglected altogether. Uncertainties arising from inadequate observational constraints on “background” $\Delta^{14}\text{CO}_2$ are less readily quantified, but may be as large as 0.5 – 1.0 ppm C_{ff} for regional-scale ($\sim 10^5$ km 2) monitoring programs (cf. Levin et al. 2010; Miller et al. 2012). These uncertainties are likely to be reduced substantially as the increasing number of recent observations are assimilated by transport models in order to represent the time-varying $\Delta^{14}\text{CO}_2$ distribution around the US.

As an example of how we apply the measurements, we present estimates of the boundary layer enhancements of C_{ff} and C_{bio} using observations obtained from vertical airborne sampling profiles off of the northeastern US (Miller et al. 2012). C_{ff} typically ranges from 0 – 7 ppm, while as much as 60% of the boundary layer CO_2 enhancement in winter is from biological respiration. We also present an updated time series of measurements from NOAA GMD’s NWR site in Colorado (3475 m asl) in order to characterize recent $\Delta^{14}\text{CO}_2$ (and the zonal $\Delta^{14}\text{CO}_2$ gradient) in the well-mixed free troposphere over the mid-latitude US.

REFERENCES

- Balter M. 2012. Using radiocarbon to go beyond good faith in measuring CO_2 emissions. *Science* 337(6093): 400–1.
- Blasing TJ, Broniak CT, Marland G. 2005. The annual cycle of fossil-fuel carbon dioxide emissions in the United States. *Tellus B* 57(2):107–15.
- Boden TA, Marland G, Andres RJ. 2010. *Global, Regional, and National Fossil-Fuel CO_2 Emissions*. Carbon Dioxide Information Analysis Center, Oak Ridge National Laboratory, US Department of Energy, Oak Ridge, Tennessee, USA.
- Ciais P, Friedlingstein P, Schimel DS, Tans PP. 1999. A global calculation of the $\delta^{13}\text{C}$ of soil respired carbon: implications for the biospheric uptake of anthropogenic CO_2 . *Global Biogeochemical Cycles* 13(2):519–30.
- Conway TJ, Tans PP, Waterman LS, Thoning KW, Kitzis DR, Masarie KA, Zhang N. 1994. Evidence for inter-annual variability of the carbon cycle from the NOAA/CMDL global air sampling network. *Journal of Geophysical Research* 99(D11):22,831–55.

- Graven HD, Gruber N. 2011. Continental-scale enrichment of atmospheric $^{14}\text{CO}_2$ from the nuclear power industry: potential impact on the estimation of fossil fuel-derived CO_2 . *Atmospheric Chemistry and Physics* 11(5):14,583–605.
- Graven HD, Guilderson TP, Keeling RF. 2007. Methods for high-precision ^{14}C AMS measurement of atmospheric CO_2 at LLNL. *Radiocarbon* 49(2):349–56.
- Graven HD, Stephens BB, Guilderson TP, Campos TL, Schimel DS, Campbell JE, Keeling RF. 2009. Vertical profiles of biospheric and fossil fuel-derived CO_2 and fossil fuel CO_2 : CO ratios from airborne measurements of $\Delta^{14}\text{C}$, CO_2 and CO above Colorado, USA. *Tellus B* 61(3):536–46.
- Graven HD, Guilderson TP, Keeling RF. 2012. Observations of radiocarbon in CO_2 at seven global sampling sites in the Scripps flask network: analysis of spatial gradients and seasonal cycles. *Journal of Geophysical Research* 117: D02303, doi:10.1029/2011JD016535.
- Hsueh D, Krakauer NY, Randerson JT, Xu X, Trumbore SE, Southon JR. 2007. Regional patterns of radiocarbon and fossil-fuel derived CO_2 in surface air across North America. *Geophysical Research Letters* 34: L02816, doi:10.1029/2006GL027032.
- International Atomic Energy Agency (IAEA). 2004. *Management of Waste Containing Tritium and Carbon-14*. Technical Report Series no. 421. Vienna: IAEA. 109 p.
- Joint Committee for Guides in Metrology (JCGM). 2008. *International Vocabulary of Metrology – Basic and General Concepts and Associated Terms*. 3rd edition. Metrology JCFGI, editor. Geneva: Bureau International des Poids et Mesures.
- Krol M, Houweling S, Bregman B, van den Broek M, Segers A, van Velthoven P, Peters W, Dentener F, Bergamaschi P. 2005. The two-way nested global chemistry-transport zoom model TM5: algorithm and applications. *Atmospheric Chemistry and Physics* 5:417–32.
- Lehman SJ, Miller JB, Turnbull JC, Southon JR, Tans PP, Sweeney C. 2011. $^{14}\text{CO}_2$ measurements in the NOAA/ESRL Global Co-operative Sampling Network: an update on measurements and data quality. In: Brand WA, editor. *15th WMO/IAEA Meeting of Experts on Carbon Dioxide, Other Greenhouse Gases and Related Tracer Measurement Techniques (Jena, GDR 7–10 September 2009)*. World Meteorological Organization Global Atmosphere Watch Report No. 194. Geneva: WMO. p 315–8.
- Levin I, Kromer B, Schmidt M, Sartorius H. 2003. A novel approach for independent budgeting of fossil fuel CO_2 over Europe by $^{14}\text{CO}_2$ observations. *Geophysical Research Letters* 30:2194, doi:10.1029/2003GL018477.
- Levin I, Kromer B. 2004. The tropospheric $^{14}\text{CO}_2$ level in mid-latitudes of the Northern Hemisphere (1959–2003). *Radiocarbon* 46(3):1261–72.
- Levin I, Hammer S, Kromer B, Meinhardt F. 2008. Radiocarbon observations in atmospheric CO_2 : determining fossil fuel CO_2 over Europe using Jungfraujoch observations as background. *Science of the Total Environment* 391(2–3):211–26.
- Levin I, Naegler T, Kromer B, Diehl M, Francey RJ, Gomez-Pelaez AJ, Steele LP, Wagenbach D, Weller R, Worthy DE. 2010. Observations and modelling of the global distribution and long-term trend of atmospheric $^{14}\text{CO}_2$. *Tellus B* 62(1):26–46.
- Miller JB, Lehman SJ, Montzka SA, Sweeney C, Miller BR, Karion A, Wolak C, Dlugokencky EJ, Southon J, Turnbull JC, Tans PP. 2012. Linking emissions of fossil fuel CO_2 and other anthropogenic trace gases using atmospheric $^{14}\text{CO}_2$. *Journal of Geophysical Research* 117: D08302, doi:10.1029/2011JD017048.
- Randerson J, Enting IG, Schuur EAG, Caldeira K, Fung IY. 2002. Seasonal and latitudinal variability of troposphere $\Delta^{14}\text{CO}_2$: post bomb contributions from fossil fuels, oceans, the stratosphere, and the terrestrial biosphere. *Global Biogeochemical Cycles* 16(4):1112, doi:10.1029/2002GB001876.
- Stohl AC, Forster A, Frank A, Seibert P, Wotawa G. 2005. Technical note: the Lagrangian particle dispersion model FLEXPART version 6.2. *Atmospheric Chemistry and Physics* 5:2461–74.
- Stuiver M, Polach HA. 1977. Discussion: reporting of ^{14}C data. *Radiocarbon* 19(3):355–63.
- Thompson MV, Randerson JT. 1999. Impulse response functions of terrestrial carbon cycle models: method and application. *Global Change Biology* 5(4):371–94.
- Thoning KW, Tans PP, Komhyr WD. 1989. Atmospheric carbon dioxide at Mauna Loa Observatory 2. Analysis of the NOAA GMCC data, 1974–1985. *Journal of Geophysical Research* 94(D6):8549–65.
- Turnbull JC, Miller JB, Lehman SJ, Tans PP, Sparks RJ, Southon J. 2006. Comparison of $^{14}\text{CO}_2$, CO , and SF_6 as tracers for recently added fossil fuel CO_2 in the atmosphere and implications for biological CO_2 exchange. *Geophysical Research Letters* 33: L01817, doi:10.1029/2005GL024213.
- Turnbull JC, Lehman SJ, Miller JB, Sparks RJ, Southon JR, Tans PP. 2007. A new high precision $^{14}\text{CO}_2$ time series for North American continental air. *Journal of Geophysical Research* 112: D11310, doi:10.1029/2006JD008184.
- Turnbull J, Rayner P, Miller J, Naegler T, Ciais P, Cozic A. 2009. On the use of $^{14}\text{CO}_2$ as a tracer for fossil fuel CO_2 : quantifying uncertainties using an atmospheric transport model. *Journal of Geophysical Research* 114: D22302, doi:10.1029/2009JD012308.
- Turnbull JC, Lehman SJ, Morgan S, Wolak C. 2010. A new automated extraction system for ^{14}C measurement in atmospheric CO_2 . *Radiocarbon* 52(3):1261–9.
- Turnbull JC, Tans PP, Lehman SJ, Baker D, Conway TJ, Chung YS, Gregg J, Miller JB, Southon JR, Zhou L-X. 2011. Atmospheric observations of carbon monoxide and fossil fuel CO_2 emissions from East Asia. *Journal of Geophysical Research* 116: D24306, doi: 10.1029/2011JD016691.